J. Fluid Mech. (2013), *vol.* 721, *pp.* 46–57.
doi:10.1017/jfm.2013.60

Study of polygonal water bells: inertia-dominated thin-film flows over microtextured surfaces

Emilie Dressaire[1,†], Laurent Courbin[2], Adrian Delancy[3], Marcus Roper[4] and Howard A. Stone[5]

[1]Department of Engineering, Trinity College, Hartford, CT 06106, USA

[2]Institut de Physique de Rennes, UMR CNRS 6251, Campus Beaulieu, Université Rennes 1, 35042 Rennes, France

[3]School of Engineering and Applied Sciences, Harvard University, Cambridge, MA 02138, USA

[4]Department of Mathematics, University of California, Los Angeles, CA 90095-1555, USA

[5]Department of Mechanical and Aerospace Engineering, Princeton University, Princeton, NJ 08544, USA

(Received 16 September 2012; revised 21 December 2012; accepted 24 January 2013; first published online 13 March 2013)

Microtextured surfaces are commonly used to study complex hydrodynamic phenomena such as spreading and splashing of liquid droplets. However, although surface topography is known to modify near-surface flow, there is no theory able to quantitatively predict the dramatic changes in dynamics of liquid spreading and splashing. Here, we investigate experimentally water bells formed on micropatterned surfaces in order to characterize the hydrodynamics of inertia-dominated flows through regular porous layers. Water bells are self-suspended catenary-shaped liquid films created when a jet impinges on a horizontal disc called an impactor. We show that the presence of micrometre-sized posts regularly arranged on the impactor results in a decrease of the water bell radius and the loss of axisymmetry as open water bells adopt polygonal shapes. We introduce a simple model that captures the main features of the inertia-dominated flow and reveals the role of the hydrodynamic interactions between neighbouring posts. In addition to their applications for tunable jet atomization, these polygonal sheets provide a paradigmatic system for understanding inertia-dominated flow in porous media.

Key words: interfacial flows (free surface), porous media, thin films

1. Introduction

When a circular liquid jet impinges normally on a flat disc of finite size, a thin liquid sheet is formed. The sheet spreads radially on the impactor before becoming free standing. The shape of the self-suspended liquid sheet results from the balance between inertial, capillary and gravitational effects. When the inertia of the liquid is greater than the surface tension force, the sheet is an open liquid bell, which is also

† Email address for correspondence: emilie.dressaire@trincoll.edu

referred to as a 'Savart sheet' (Savart 1833*a*,*b*). Upon decrease of the jet velocity, the curved sheet progressively closes onto the impactor forming a closed liquid bell.

In his pioneering work, Savart documented the formation of stable liquid sheets and bells (Savart 1833*a*,*b*). The catenary shape of stable water bells was first derived by Boussinesq (1869*a*,*b*). Further, Lance & Perry (1953) determined the shape of a bell when the air pressure inside the closed structure is not negligible. Savart also reported the various shapes adopted by the free-standing liquid sheet when the diameters of the jet and impactor are varied (Savart 1833*a*,*b*). The complex behaviour evidenced has since prompted several theoretical and experimental studies on the stability and shape of water bells. For example, Clanet (2001) studied the stability of the bells, Buckingham & Bush (2001) observed the formation of polygonal water bells when a liquid more viscous than water is used and Lhuissier & Villermaux (2012) derived a model that explains the formation of singular crumpled bells for certain values of the pressure difference across the liquid sheet. Since the disintegration of open bells or Savart sheets into droplets has numerous engineering applications, this phenomenon of atomization has been the focus of recent studies (Bremond, Clanet & Villermaux 2007; Ashgriz 2011).

Our goal is to explore how regular microtexturing of the impactor influences the shape and stability of water bells. Previous studies on splashing (Courbin, Bird & Stone 2006; Xu 2007; Tsai *et al.* 2011) and hydraulic jumps (Dressaire *et al.* 2010) have exploited the interactions between micrometre-scale topological features and thin liquid films formed when a drop or a jet impinges on the surface at high velocities. In our experiments with micropatterned impactors, the flow along the surface occurs through the dilute porous microstructure and the motion is dominated by inertia. This regime is not well characterized at the pore scale, and because of the small-scale structures and high flow speeds, direct measurement of the velocity, e.g. by particle image velocimetry (PIV), poses challenges. Here we use the geometry of a water bell to measure indirectly the velocity of the fluid as it exits the porous microstructure and imparts a polygonal shape to the water bell.

The paper is organized as follow. A description of the experimental set-up is provided in § 2. In § 3, we present our experimental results: we show that open water bells adopt polygonal shapes with preferred droplet emission sites located at the vertices of the created polygonal structures. In § 4, we introduce a model that captures the behaviour of the flow on the micropatterned surfaces and we conclude in § 5.

2. Experimental set-up

To investigate the role of the surface roughness, we utilize most features of an experimental set-up developed to study water bells (Clanet 2007). A schematic of our experimental set-up is presented in figure 1. The liquid is initially stored in a tank pressurized at 276 kPa. When we open the outlet valve, the liquid flows into a nozzle of diameter $D_0 = 2.5$–3.5 mm and forms a jet. Two flow meters (AALBORG) mounted in parallel control and measure the flow rate Q of the jet allowing variations between $0.5 \leqslant Q \leqslant 2.5$ L min^{-1} with a resolution of 0.15 L min^{-1}. Liquids including water and isopropanol are used, as well as mixtures of these two fluids.

We define two non-dimensional parameters to characterize a liquid jet. The Reynolds number $Re = U_0 D_0/\nu$ represents the ratio of the inertia to the viscous forces. The Weber number $We = \rho U_0^2 D_0/\gamma$ represents the ratio of the kinetic energy to the surface energy, where ρ is the liquid density, γ the surface tension, ν the kinematic viscosity, D_0 the jet diameter and $U_0 = 4Q/(\pi D_0^2)$ the jet velocity.

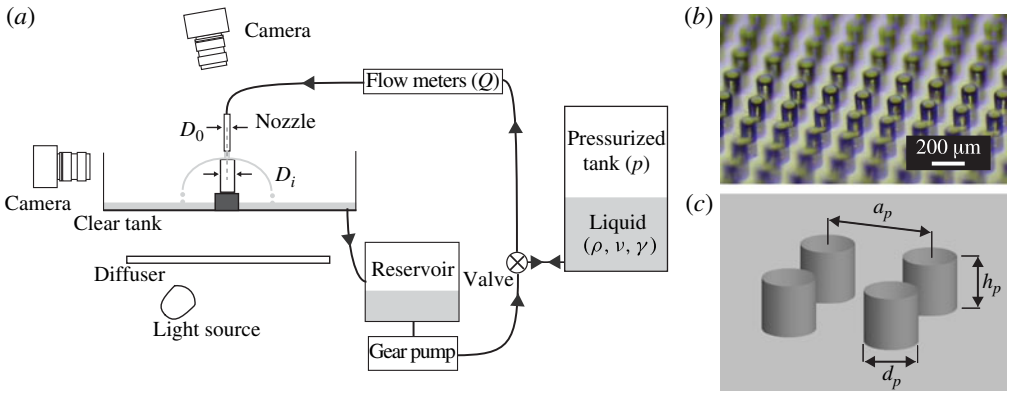

FIGURE 1. (Colour online) (*a*) Schematic of the experimental set-up. The liquid flows in a closed circuit indicated by the black arrows. The fluid is pushed through a nozzle forming a jet that impinges on the impactor. A water bell is created. The liquid is collected in a clear tank, flows in a reservoir and is pumped back into the pressurized tank. Other experimental parameters are: pressure p, flow rate Q and liquid properties (γ, ν, ρ). (*b*) Optical microscope image of a square lattice of cylindrical posts. (*c*) Schematic representation of the unit cell of a square lattice, defining the parameters of the posts (d_p, h_p) and the lattice spacing a_p.

The impactor is a clear acrylic cylinder with diameter $D_i = 0.6$–5 cm. We define the diameter ratio $X = D_i/D_0$. The impacted surface is a smooth or microtextured circular sheet of transparent PDMS (polydimethylsiloxane silicone elastomer, SYLGARD 184) of thickness 2–3 mm and diameter D_i. The surface texture consists of an array of cylindrical microposts regularly arranged in a lattice of typical length scale of 200 μm (see figure 1*b*). We fabricate the micropatterns using standard soft lithography techniques (McDonald & Whitesides 2002) and use different molds to vary the lattice symmetry (hexagonal and square) and geometric parameters. The diameter of the cylindrical posts is fixed at $d_p = 100$ μm, while the height is varied in the range $h_p = 23$–88 μm. The spacing between posts a_p spans from 200 to 400 μm (see figure 1*c*).

Upon impact on the PDMS surface, the liquid flows radially and forms a liquid bell. In a typical experiment, the steady shape of the stable liquid sheet is recorded while the flow rate of the jet is decreased from its maximum value to avoid hysteresis effects associated with the detachment of the sheet from the impactor as Q increases. The shape of the bell is captured with two cameras (Edmund Optics, *EO* 0413*M*). Two geometrical features are needed to describe the shape of a water bell: (i) the angle of ejection from the impactor φ_0; and (ii) the maximum radial extent of the bell R_B (see figure 2). To determine R_B, a camera is located above the impactor. To capture φ_0, a second camera is placed perpendicular to the axis of the jet. The video data is analysed using custom-written Matlab software. The value of R_B is defined by averaging over 200 values of the position of the rim of the open bells and the equatorial radii of closed bells.

3. Experimental results

We begin with brief remarks about the shape of water bells formed on smooth impactors before discussing the case of microtextured impactors (see figure 3). In the experiments, water jets with $D_0 = 3$ mm and $U_0 = 2.3$–4.2 m s^{-1} impinge on an

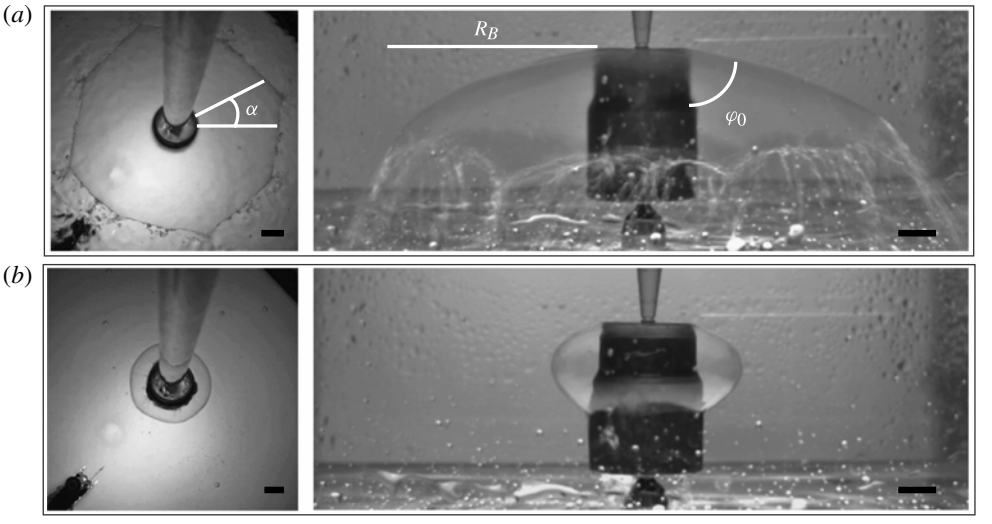

FIGURE 2. Top and side views of representative water bells. (*a*) Open water bell, $U_0 = 4\ \mathrm{m\ s^{-1}}$, $We = 680$ and $Re = 1.2 \times 10^4$. (*b*) Closed water bell, $U_0 = 2.3\ \mathrm{m\ s^{-1}}$, $We = 250$ and $Re = 7.1 \times 10^3$. Jets of isopropanol/water mixture (0.5 vol.% of isopropanol) impinge on a square lattice of microposts with $a_p = 200\ \mu\mathrm{m}$ and $h_p = 55\ \mu\mathrm{m}$. Here $D_0 = 3$ mm, $D_i = 2.5$ cm. Scale bars: 1 cm.

impactor of diameter $D_i = 2.5$ cm. At large velocities, the liquid sheet is unstable and its rim blurry (data not shown). Below a critical flow rate, the liquid sheet or open bell adopts a stable, nearly conical shape with droplets emitted uniformly along the rim. In what follows we will focus on flow rates below this critical value. Initially, R_B and φ_0 decrease and, eventually, the liquid structure closes on the impactor to form a closed water bell.

Water bells formed when jets of different flow rates impinge on a micropatterned impactor show similar characteristics but are clearly differentiated by their non-axisymmetric shapes at larger flow rates. Below a critical flow rate, the liquid sheet formed on a micropatterned impactor is stable with well-defined rims. As the flow rate decreases, the bell shrinks and the curvature of the sheet increases. Beyond these similarities, three features of the water bells differ between the cases of smooth and rough impactors. First, for a fixed flow rate, the water bell formed on a micropatterned surface is smaller than that formed on a smooth surface. Second, stable open bells formed on a microtextured surface are not axisymmetric, but rather are polygonal structures whose shapes are defined by the symmetry of the lattice. Figure 3 shows that an octagonal shape is produced by the four-fold symmetry of a square lattice and an hexagonal shape is created by the six-fold symmetry of a hexagonal lattice. The vertices of these polygonal shapes are directed along the principal axes of the lattices and, in the case of square lattices, along diagonals as well. The vertices are located in the regions of maximum velocity, i.e. along the directions of the lattice with least resistance to the water flow. We note that the polygonal shape rotates along with the impactor (data not shown). Using figures 2(*a*) and 3(*a*), we compare the effects of the flow rate and surface tension on the shape of the polygonal structure. For any liquid, the shape of the polygonal open bell is independent of Q, as can be seen in figure 3(*a*). However, the sharpness of the polygonal shape depends on the surface tension of the

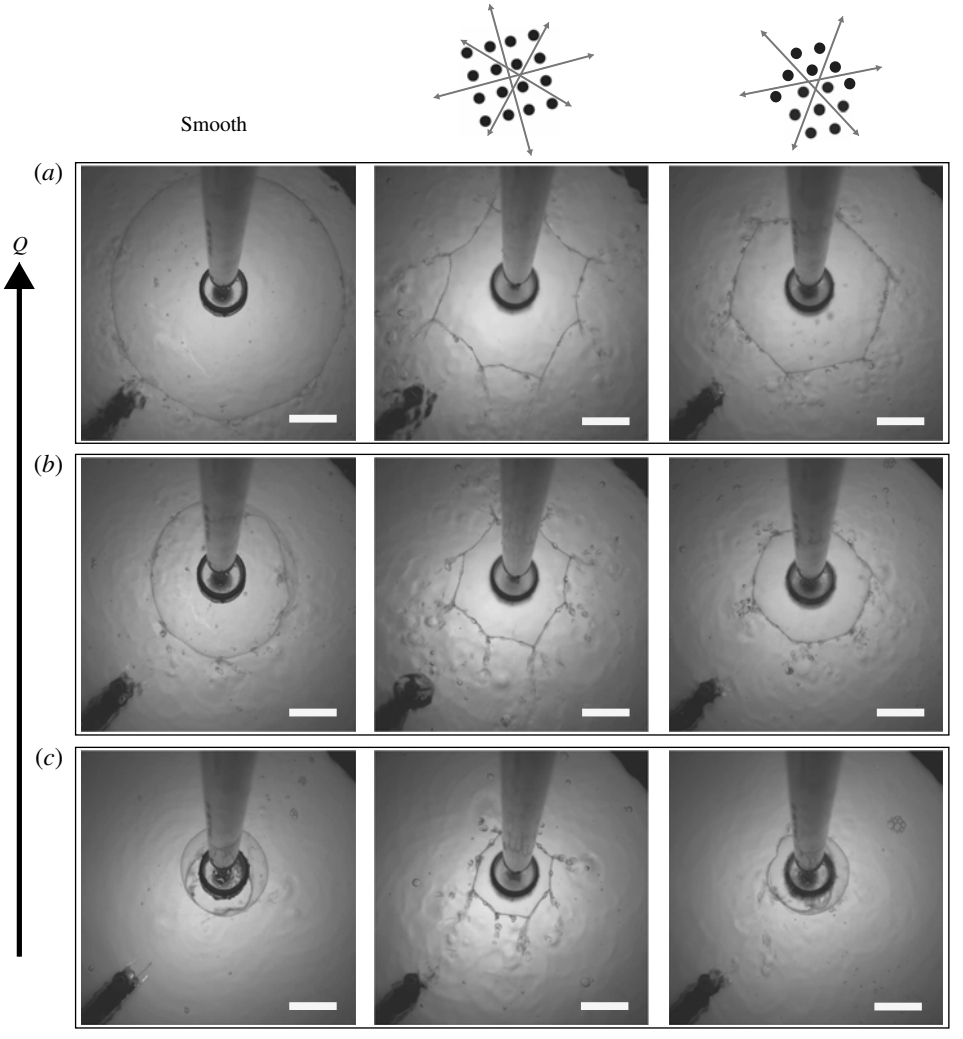

FIGURE 3. Evolution of the shape of the water bell with the jet flow rate upon impact on three different surfaces. From left to right column: smooth surface, square lattice ($a_p = 200$ μm, $h_p = 55$ μm) and hexagonal lattice ($a_p = 200$ μm, $h_p = 51$ μm). The flow rate decreases from top to bottom row with: (*a*) $We = 550$ and $Re = 1.1 \times 10^4$; (*b*) $We = 390$ and $Re = 9.2 \times 10^3$; (*c*) $We = 230$ and $Re = 7.1 \times 10^3$. Here $D_0 = 3$ mm and $D_i = 2.5$ cm. Scale bars: 2.5 cm.

liquid. Finally, most of the droplets emitted from the rim of the polygonal bells are ejected at the vertices.

Before comparing the shape of water bells formed on smooth and micropatterned surfaces, we recall the theoretical dependence of the structure of a water bell on the flow rate of a jet impinging on a smooth impactor. Upon impact, the liquid spreads radially over the solid surface: the sheet thickness $h(r)$ and liquid velocity averaged over the thickness of the sheet $U(r)$ are decreasing functions of the radial distance r due to viscous losses associated with the development of a boundary layer of thickness $\delta(r)$ at the solid surface (Watson 1964). At the edge of the impactor, the average

velocity U_e, also called the ejection velocity, and the film thickness h_e depend on Re and X (Clanet 2001):

$$\text{For } X \leqslant 0.37Re^{1/3} \qquad \text{For } X > 0.37Re^{1/3} \tag{3.1}$$

$$\delta\left(\frac{D_i}{2}\right) \approx 1.83\, D_0\sqrt{\frac{X}{Re}} \qquad \delta\left(\frac{D_i}{2}\right) \approx \frac{1.21D_0}{Re}\frac{X^3 + 8\,(Re/3)^3}{X} \tag{3.2}$$

$$h_e \approx \frac{D_0}{4X} + 0.39\,\delta\left(\frac{D_i}{2}\right) \qquad h_e \approx \delta\left(\frac{D_i}{2}\right) \tag{3.3}$$

$$\widetilde{U_e} \approx \sqrt{\frac{1-\left(X/Re^{1/3}\right)^{3/2}}{1+2.82\left(X/Re^{1/3}\right)^{3/2}}} \qquad \widetilde{U_e} \approx 0.81\frac{1}{1+3.5\left(X/Re^{1/3}\right)^3} \tag{3.4}$$

where $\widetilde{U}_e = U_e/U_0$ is the reduced ejection velocity. For example, when a water jet ($D_0 = 3$ mm) impinges on an impactor ($D_i = 2.5$ cm) with a velocity varying from 1.2 to 6 m s^{-1}, the film thickness h_e decreases from 195 to 141 μm while $\widetilde{U_e}$ increases from 0.52 to 0.71. The thickness of the viscous boundary layer is maximum at the edge of the impactor where $\delta(D_i/2)$ decreases from 195 to 133 μm as Q increases. When the sheet leaves the impactor, the velocity of the fluid remains equal to U_e. The curved shape of the bell is obtained by balancing capillary, gravity and 'centrifugal' forces (Taylor 1959; Clanet 2007). In this study, we do not consider the influence of a pressure difference across the liquid sheet as very few bells obtained experimentally exhibited a perfectly closed structure allowing for pressure equalization. We estimate the magnitude of the forces for the range of parameters studied: gravity is negligible compared with the centrifugal force ($g\,R_B/U_e^2 = O(10^{-2})$ with $R_B \approx 10^{-2}$ m) and to the capillary force ($\rho\, g\, R_B\, h_e/\gamma = O(10^{-1})$). At high Weber numbers, assuming that $\widetilde{U_e} \approx 1$, and balancing only capillary and inertial forces give a relationship between the radius of the bell and the angle of ejection (Clanet 2007):

$$\frac{2R_B}{D_0\,(1-\cos\varphi_0)} \approx \frac{We}{8}. \tag{3.5}$$

To compare the experimental values of the liquid bell radius with (3.5), we plot the scaled radius, defined as $2\,R_B/D_0\,(1-\cos\varphi_0)$, as a function of $We/8$ (see figure 4*a–b*). The linear dependence of the scaled radius on the Weber number that is observed on smooth impactors is lost upon introduction of surface roughness. In figure 4(*a*), we present experimental values of the scaled bell radius corresponding to bells created on smooth impactors while varying the surface tension γ and the geometry of the system X. The experimental data collapse onto a line of slope 1 for $We < 800$, as the bells are closed. Above this critical value, the liquid sheets disintegrate into droplets before reaching the solution of (3.5). In figure 4(*b*), we present the scaled radius of bells formed on microtextured impactors with different surface roughness, fluid properties, and diameter ratios. These data collapse over a small range of We and both open and closed bells have smaller radii than for smooth impactors. As the roughness is increased, for example by increasing h_p or decreasing a_p, the radius decreases. When the impactor diameter D_i or the jet velocity is drastically reduced the radii of the bells on micropatterned and smooth impactors are comparable (see ● and $We/8 \leqslant 50$ in figure 4*b*).

These observations show that the presence of microposts on the impactor reduces the bell radius: this response results from a reduction of the ejection velocity. For

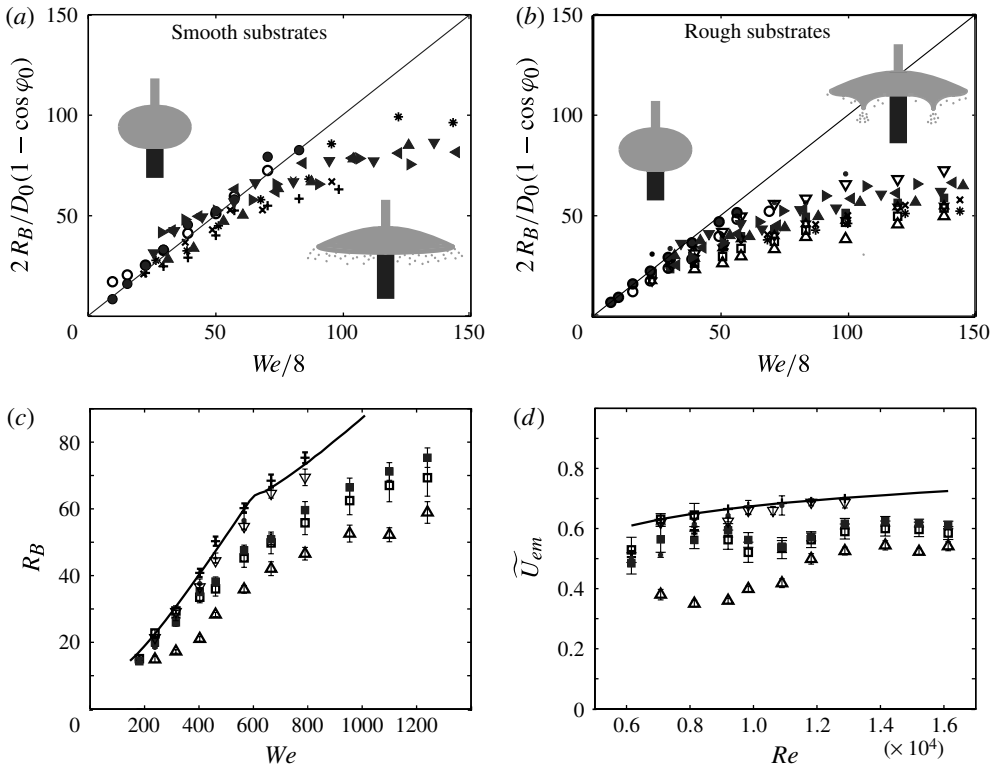

FIGURE 4. Evolution of the scaled bell radius with the Weber number of the jet impacting (*a*) smooth and (*b*) rough surfaces. Experimental conditions to study the effects of surface topography, X and γ: water jets ($D_0 = 3$ mm) impinge on impactors ($D_i = 2.5$ cm) covered with different surfaces: +, smooth and square lattices with (h_p, a_p) in μm; □, (55, 200); ■, (55, 200); ·, (55, 400); ▷, (61, 200); △, (88, 200); ▽, (23, 200). The properties of the jet and size of the impactor are also varied while keeping surface properties identical (smooth surface in (*a*) and surface covered by a square lattice (55, 200) in (*b*)). For $\gamma \approx 72$ mN m^{-1}: ○, $D_0 = 3$ mm and $D_i = 1.25$ cm; ●, $D_0 = 3$ mm and $D_i = 0.6$ cm; ∗, $D_0 = 2.5$ mm and $D_i = 2.5$ cm; ×, $D_0 = 2$ mm and $D_i = 2.5$ cm. For $D_0 = 3$ mm and $D_i = 2.5$ cm, ▲, $\gamma \approx 68$ mN m^{-1}; ▼, $\gamma \approx 63$ mN m^{-1}; ▶, $\gamma \approx 56$ mN m^{-1}; ◀, $\gamma \approx 49$ mN m^{-1}. The insets in (*a,b*) are schematics of the shape of the water bells observed at low and high We. (*c*) Comparison between experimental water bell radii and (3.6)–(3.7), represented by the continuous line. Symbols are identical to those in (*a,b*). The error bars represent the standard deviation of R_B, divided by two. (*d*) Estimate of $\widetilde{U}_{em}$ as a function of Re. The continuous line corresponds to (3.4). Symbols are identical to those in (*a,b*). The error bars represent the standard deviation of $\widetilde{U}_{em}$.

each value of the bell radius, we seek to determine the corresponding ejection velocity. For smooth impactors, the value of the ejection velocity U_e as a function of Re can be accurately estimated by accounting for viscous losses on the impactor (Watson 1964; Clanet 2001). To determine the bell radius, we differentiate between the low We region ($We \lesssim 600$), in which the water bells are closed (Clanet 2007) and the high We region, in which the water bells are open. When a liquid bell is open, its rim disintegrates into droplets before the bell closes and the radius of the sheet depends on the energy dissipated in the drop formation: $E_{drop} = x E_{jet}$, where $x = 0.1$–0.2

(Clanet & Villermaux 2002; Bremond 2003). The bell radius is therefore defined by two equations:

$$R_{B\,closed} \approx \frac{We\,\widetilde{U}_e}{8}\frac{D_0}{2}(1-\cos\varphi_0)+\frac{D_i}{2}\cos\varphi_0 \tag{3.6}$$

$$R_{B\,open} \approx \frac{We\,\widetilde{U}_e}{8}\frac{D_0}{2}\left(1-\frac{\sqrt{x-12/We^{2/3}}}{\widetilde{U}_e}\right) \tag{3.7}$$

where $\cos\varphi_0 - 0.1 = (8X/We)\sin\varphi_0$. Figure 4(*c*) shows that a good fit of our experimental data for a smooth impactor is obtained for $x = 0.18$. We use (3.6) and (3.7) established for a smooth substrate to determine the values of the ejection velocity averaged over the angle α (see figure 2) and denoted by $\widetilde{U}_{em}$ for rough impactors (see figure 4*d*).

Comparing the ejection velocities from smooth and rough impactors reveals that the viscous dissipation associated with the growth of a boundary layer is not responsible for the formation of polygonal bells on rough impactors. Indeed only $\widetilde{U}_{em}$ corresponding to small diameter or low roughness impactors are comparable with the predicted values. For all other micropatterned impactors, $\widetilde{U}_{em}$ remains almost constant for the range of Reynolds numbers explored. Here $\widetilde{U}_{em}$ decreases as the roughness of the impactor increases and is reduced by up to 30 % compared with the value obtained for a smooth impactor.

4. The role of hydrodynamic interactions between posts

To understand how the thin-liquid film interacts with the microtextured impactor, we model the inertia-dominated flow through the lattice of microposts. In our experiments, when the liquid enters the network of posts, the Reynolds number $Re_{post} = U_0\,d_p/\nu$ varies between 200 and 500. As discussed above, the distance over which the viscous boundary layer invades a film of thickness 100 μm is comparable with the radius of the impactors. This feature indicates that inertial effects are dominant not only in the thin film but in the flow through the micropatterns at least close to the location of the jet impact. We assume that the flow anisotropy is associated with the inertia-dominated flow through the posts.

Inertial effects in porous media are often described with a non-local Darcy-like equation in which the inertial effects are averaged and isotropic (Ergun 1952; Koch & Ladd 1997). To describe the local interactions between the posts and the flow and capture the anisotropy of the flow, we assume that the dissipation associated with the development of viscous boundary layers is negligible compared with the drag on the microposts. For Reynolds numbers of the order of 300, inertial effects are considered dominant and we model the drag on each cylindrical post by a point force $D = (C_D/2)\,\rho\,u^2\,A_p$ where $A_p = h_p\,d_p$ is the cross-sectional area of a post, u the typical velocity of the liquid in the microstructure and C_D the drag coefficient of a micropost. As a first approximation, we neglect the confined geometry and assume that $C_D \approx 1.4$ (Batchelor 2010). The location and orientation of the point forces is prescribed by the lattice structure of the impactor. We balance momentum for a sector of a disc of depth $h(r)$ equal to the thickness of the liquid layer and of radius varying between $D_0/2$ and $D_i/2$. We know that the flow is on average radial, thus u the velocity and the volume force are radially directed. We explicitly model the structure of the microtextured layer.

Specifically, in the steady state,

$$0 = \int_A \rho\, u^2\, \mathrm{d}A - \frac{C_D}{2}\, \rho\, d_p\, h_p \sum_{\boldsymbol{r_i}} u\,(\boldsymbol{r_i})^2 \tag{4.1}$$

with dA the elementary surface area normal to the radial direction. The volume force is a distribution of point forces located at the positions of the microposts ($\boldsymbol{r_i}$) in the sector of central angle dθ, centred on θ.

We use mass conservation in the sheet to define $h(r) = R_0^2\, U_0/[2\, r\, U(r)]$ and solve for the steady radial flow:

$$\widetilde{U_e}(\theta, \mathrm{d}\theta) \approx 1 - \frac{4\, C_D\, d_p\, h_p}{D_0^2\, \mathrm{d}\theta} \sum_{\boldsymbol{r_i}(\theta)} \frac{u\,(\boldsymbol{r_i})^2}{U_0^2}. \tag{4.2}$$

To define the dimensionless ejection velocity $\widetilde{U_e}(\theta)$, we solve for $\widetilde{U_e}(\theta, \mathrm{d}\theta)$ for an increment of $\mathrm{d}\theta = \pi/180$ using an iterative method over increasing values of r_i. Each value of the ejection velocity is averaged over a sector of central angle $\arctan(2a_p/D_0) \approx 7\pi/180$ which contains between 5 and 15 microposts.

The flow interaction with each post produces ejection velocities far smaller than that observed in our experiments. For example, for a square lattice with parameters $a_p = 200$ μm and $h_p = 55$ μm, the theory predicts $\widetilde{U_{em}} = 0.2$ whereas the experimental value is ∼0.6. This approach also fails to predict the angular dependence correctly. Indeed along the axes of the lattice, the linear density of posts is the greatest, the total drag force is a maximum and the predicted ejection velocity is a minimum. By contrast, the experiments show that the bell radius is a maximum, which corresponds to a maximum value of $\widetilde{U_e}$.

These experimental results suggest that lattices having a higher density of posts present a smaller total drag force, which indicates that the posts are interacting hydrodynamically. Indeed, for values of Reynolds number ∼300, the size of the wake of a circular cylinder is several times its diameter (Batchelor 2010). Numerical studies on pairs of cylinders in tandem show that, for a spacing $a_p \sim 2d_p$, the drag coefficient of the second post is considerably lower than the drag coefficient of the first post and can even be negative (Sharman *et al.* 2005). To improve our model, we next consider that all of the posts located in the wake of another post situated closer to the impinging jet contribute a negligible drag: a row of posts acts as a single post, with all of the posts behind this first post shielded by its separated wake. The positions of these first posts are determined numerically (see figure 5*a,b* for the square and the hexagonal lattices, respectively). We compute the ejection velocity $\widetilde{U_e}(\theta)$ using the distribution of first posts. The results for a square lattice of microposts with parameters $a_p = 200$ μm, and $h_p = 55$ μm are represented in figure 5(*c*) by a solid line. $\widetilde{U_e}$ is independent of the average velocity of the jet which is in agreement with our experimental results (see □ in figure 4*d*). The predicted average reduced ejection velocity is equal to $\widetilde{U_{em}} = 0.63$ which is comparable with the experimental value ($\widetilde{U_{em}} \approx 0.58$). The angular dependence of $\widetilde{U_e}$ is well captured by the model with the ejection velocity reaching maxima along the four axes and four diagonals of a square lattice and along the six axes of a hexagonal lattice (see figure 5*c,d*). Note that this model predicts the flow velocity that controls the radius of the polygonal sheet according to (3.6) and (3.7). The polar representation of $\widetilde{U_e}$ allows us to compare the results obtained for different post heights. As h_p increases, $\widetilde{U_{em}}$ decreases and the ratio

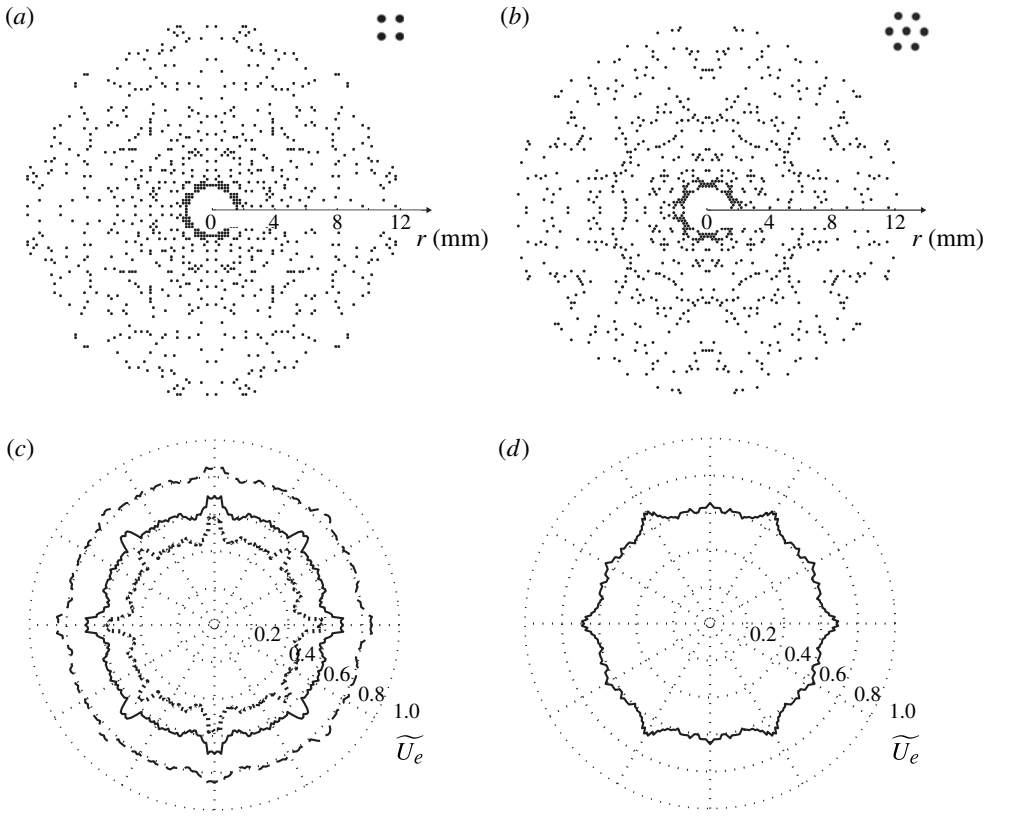

FIGURE 5. Distribution of the point forces on an impactor of diameter $D_i = 2.5$ cm, impacted by a jet of diameter $D_0 = 3$ mm. The symmetry of the modelled lattices is (*a*) square and (*b*) hexagonal with $a_p = 200$ μm and $h_p = 55$ μm. Each point corresponds to the position of a 'first post' met in the radial direction. Polar representation of the predicted value of $\widetilde{U_e}$ for (*c*) square lattices: $a_p = 200$ μm and $h_p = 23$ μm (dashed line), $a_p = 200$ μm and $h_p = 55$ μm (continuous line), $a_p = 200$ μm and $h_p = 88$ μm (dotted line); (*d*) hexagonal lattice: $a_p = 200$ μm and $h_p = 55$ μm.

of the maximum to the average ejection velocity increases, which is consistent with our experimental data (see ∇, □ and △ in figure 4*d*). Similarly the model captures the influence of the impactor diameter D_i and lattice spacing a_p, within the range studied here. This approach, which relies on 'perfect wake interaction' between posts, would not accurately describe the flow in more dilute porous micropatterns or at lower velocity, as the development of a viscous boundary layer on the lower surface of the impactor could no longer be neglected (Dressaire *et al.* 2010).

5. Conclusion

Using liquid jets impacting solid substrates, we have investigated the flows of thin films of liquids over centimetre-sized microtextured surfaces, the characteristic length scale of the surface roughness, typically 100 μm, being of the order of the film thickness. As a result, the liquid bells formed exhibit macroscopic geometrical features that reflect the geometry of the lattice, e.g. the polygonal structure of the

open bells and uneven pattern of droplet emission along the rim. We characterize experimentally the structure of water bells formed on micropatterned surfaces. In addition, we use the hydrodynamics of a free-standing liquid sheet to estimate the velocity of the liquid as it leaves the impactor, allowing pore-averaged flows to be measured. We describe the interactions between the substrate and the inertia-dominated flow and show that the reduction in velocity is due to the drag force exerted by the microposts. The effective number of posts that the sheet interacts with is reduced by the hydrodynamic interactions between neighbouring posts. The anisotropy of the ejection velocity is also responsible for the localized emission of droplets at the vertices of the polygonal shapes observed in our experiments. We note that liquid sheets formed on smooth impactors have found applications in atomization processes (Ashgriz 2011) but generally emit droplets isotropically (Juarez *et al.* 2012). The targeted emission of droplets by microtextured impactors along symmetry lines may lend themselves to applications requiring more control over the emission process.

Acknowledgements

We thank the Harvard MRSEC and NSF (CBET 0854046) for supporting this research. We also thank E. Villermaux for his input to the experimental set-up. M.R. is supported by a fellowship of the Alfred P. Sloan Foundation.

REFERENCES

ASHGRIZ, N. 2011 *Handbook of Atomization and Sprays: Theory and Applications*. Springer.

BATCHELOR, G. K. 2010 *An Introduction to Fluid Dynamics*. Cambridge University Press.

BOUSSINESQ, J. 1869*a* Théories des expériences de Savart, sur la forme que prend une veine liquide apres s'être choquée contre un plan circulaire i. *C. R. Acad. Sci. Paris* **69**, 45–48.

BOUSSINESQ, J. 1869*b* Théories des expériences de Savart, sur la forme que prend une veine liquide apres s'être choquée contre un plan circulaire ii. *C. R. Acad. Sci. Paris* **69**, 128–132.

BREMOND, N. 2003 Stabilité et Atomisation Des Nappes Liquides. PhD thesis, Université de Provence, Aix-Marseille I.

BREMOND, N., CLANET, C. & VILLERMAUX, E. 2007 Atomization of undulating liquid sheets. *J. Fluid Mech.* **585**, 421–456.

BUCKINGHAM, R. & BUSH, J. W. M. 2001 Fluid polygons. *Phys. Fluids* **13**, S10.

CLANET, C. 2001 Dynamics and stability of water bells. *J. Fluid Mech.* **430**, 111–147.

CLANET, C. 2007 Waterbells and liquid sheets. *Annu. Rev. Fluid Mech.* **39**, 469–496.

CLANET, C. & VILLERMAUX, E. 2002 Life of a smooth liquid sheet. *J. Fluid Mech.* **462**, 307–340.

COURBIN, L., BIRD, J. C. & STONE, H. A. 2006 Splash and anti-splash: observation and design. *Chaos* **16**, 41102.

DRESSAIRE, E., COURBIN, L., CREST, J. & STONE, H. A. 2010 Inertia dominated thin-film flows over microdecorated surfaces. *Phys. Fluids* **22**, 073602.

ERGUN, S. 1952 Fluid flow though packed columns. *Chem. Engng Prog.* **48**, 89–94.

JUAREZ, G., GASTOPOULOS, T., ZHANG, Y., SIEGEL, M. L. & ARRATIA, P. E. 2012 Splash control of drop impacts with geometric targets. *Phys. Rev.* E **85**, 026319.

KOCH, D. L. & LADD, A. J. C. 1997 Moderate Reynolds number flows through periodic and random arrays of aligned cylinders. *J. Fluid Mech.* **349**, 31–66.

LANCE, G. N. & PERRY, R. L. 1953 Water bells. *Proc. Phys. Soc.* B **66**, 1067–1072.

LHUISSIER, H. & VILLERMAUX, E. 2012 Crumpled water bells. *J. Fluid Mech.* **693**, 508–540.

MCDONALD, J. C. & WHITESIDES, G. M. 2002 Poly(dimethylsiloxane) as a material for fabricating microfluidic devices. *Acc. Chem. Res.* **35**, 491–499.

SAVART, F. 1833*a* Mémoire sur le choc d'une veine liquide lancée contre un plan circulaire. *Ann. Chim.* **54**, 56–87.

SAVART, F. 1833*b* Suite du mémoire sur le choc d'une veine liquide lancée contre un plan circulaire. *Ann. de Chim.* **54**, 113–145.

SHARMAN, B., LIEN, F. S., DAVIDSON, L. & NORBERG, C. 2005 Numerical predictions of low Reynolds number flows over two tandem circular cylinders. *Intl J. Numer. Meth. Fluids* **47**, 423–447.

TAYLOR, G. 1959 The dynamics of thin sheets of fluid. I. Water bells. *Proc. R. Soc. Lond.* A **253** (1274), 289–295.

TSAI, P., HENDRIX, M. H. W., DIJKSTRA, R. R. M., SHUI, L. & LOHSE, D. 2011 Microscopic structure influencing macroscopic splash at high Weber number. *Soft Matt.* **7**, 11325.

WATSON, E. J. 1964 The radial spread of a liquid jet over a horizontal plane. *J. Fluid Mech.* **20**, 481–499.

XU, L. 2007 Liquid drop splashing on smooth, rough, and textured surfaces. *Phys. Rev.* E **75**, 056316.